

Parameter-free Clustering of Free Energy Landscapes with Gaussian Mixtures

Annie M. Westerlund and Lucie Delemotte*

Science for Life Laboratory, Department of Applied Physics, KTH Royal Institute of Technology, Box 1031, SE-171 21 Solna

E-mail: lucie.delemotte@scilifelab.se

Abstract

Free energy landscapes provide insights into conformational ensembles of biomolecules. In order to analyze these landscapes and elucidate mechanisms underlying conformational changes, there is a need to extract metastable states with limited noise. This has remained a formidable task, despite a plethora of existing clustering methods.

We propose a novel method for extracting well-defined core states from free energy landscapes. The method is based on a Gaussian mixture free energy estimator, and exploits the shape of the estimated density landscape. The core states that naturally arise from the clustering allow for detailed characterization of the conformational ensemble in a parameter-free way. The clustering quality is evaluated on three toy models with different properties, where the method is shown to consistently outperform other conventional clustering methods. Finally, the method is applied to a temperature enhanced molecular dynamics simulation of Ca²⁺-bound Calmodulin. Through the free energy landscape, we discover a pathway between a canonical and a compact state, revealing conformational changes driven by electrostatic interactions.

1 Introduction

Gaussian mixture models provide accurate estimates of free energy landscapes¹. Determining core states within a protein’s free energy landscape is key to obtaining important biological insights. However, extracting such states from molecular dynamics (MD) simulations with conventional clustering methods is far from straightforward.

First of all, we are interested in the metastable configurations at free energy minima, the so-called core states. Since proteins move continuously as they explore free energy landscapes, it is difficult to assess an exact state boundary. Moreover, configurations on transition pathways between metastable states generally contribute to noise when characterizing these states. On top of this, the original data is high dimensional, and the necessary dimensionality reduction results in poorly separated states. Finally, the number of metastable core states is typically not known a priori. Thus, to robustly characterize states without any knowledge of the conformational ensemble, we need a clustering method that is solely based on the data.

Many popular clustering methods are based on simple geometric criteria²⁻⁵. K-means and agglomerative-Ward, for example, attempt to minimize the within-cluster variance. They work very well on datasets with well-separated spherical clusters, but fail when these assumptions are not met. Spectral clustering⁶, on the other hand, can accurately assign labels to nonconvex clusters by performing spectral embedding prior to K-means clustering. The spectral embedding involves learning the data manifold of local neighborhoods around data points. Choosing the size of this neighborhood, however, is not trivial, and greatly affects the clustering quality.

In general, geometric clustering methods assign labels to all points and may not accurately identify the boundary between states at the free energy barrier, which leads to noisy state definitions. An idea is to use the data density to identify clusters and make cuts at free energy barriers⁷⁻⁹. Although this idea seems simple, there are still problems to address. Density peaks, for example, uses local basis functions for estimating the density. This makes overfitting more likely, especially in sparse regions. Moreover, the method assumes largely

separated cluster centers with significantly high density. Metastable states in a hierarchical protein free energy are, on the contrary, not necessarily of the same size, nor of high density. Gaussian mixture model (GMM)^{10,11} is optimized on the full dataset, but instead rests on the assumption of Gaussian shaped clusters. The number of Gaussian components is usually chosen based on how well the model fits the density, which does not necessarily coincide with the number of clusters. Therefore, methods for merging components in GMM to find the correct number of clusters have been proposed¹². Another problem is the definition of core state boundaries, which typically are determined with a chosen cutoff^{7,9}. Such a cutoff does, however, not account for the possibly varying structure and shape of a protein free energy landscape.

In this paper, we propose a parameter-free clustering method that makes minimal assumptions about cluster shapes or dataset structure. We call it the inflection core state (InfleCS) clustering. It is based on estimated density landscapes from Gaussian mixtures models. The functional form of the landscape is exploited to extract well-defined free energy core states. We show that InfleCS clustering outperforms conventional methods on three different types of toy models, and use it to characterize the conformational landscape spanned by molecular simulations of Ca²⁺-bound Calmodulin.

2 Clustering Gaussian mixture free energy landscapes

The InfleCS clustering method extends a previously published Gaussian mixture model free energy estimator¹. The free energy along collective variables (CVs), $x \in \mathbb{R}^{N_{\text{dims}}}$, is given by the inverse Boltzmann distribution,

$$G(x) = -k_B T \log \rho_{\mathbf{a}, \boldsymbol{\mu}, \boldsymbol{\Sigma}}(x), \tag{1}$$

where $\rho_{\mathbf{a}, \boldsymbol{\mu}, \boldsymbol{\Sigma}}(x)$ is a Gaussian mixture density at x .

2.1 Gaussian mixture model density estimation

A Gaussian mixture density is described by a sum of Gaussians with individual amplitudes, $\mathbf{a} := (a_i)_{i=1}^{N_{\text{basis}}}$, means $\boldsymbol{\mu} := (\mu_i)_{i=1}^{N_{\text{basis}}}$ and covariances $\boldsymbol{\Sigma} := (\Sigma_i)_{i=1}^{N_{\text{basis}}}$,

$$\rho_{\mathbf{a}, \boldsymbol{\mu}, \boldsymbol{\Sigma}}(x) = \sum_{i=1}^{N_{\text{basis}}} a_i \mathcal{N}(x | \mu_i, \Sigma_i), \quad (2)$$

where $\mathcal{N}(x | \mu_i, \Sigma_i) = \frac{1}{\sqrt{(2\pi)^{N_{\text{dims}}|\Sigma_i|}}} e^{\hat{f}_i}$ is a Gaussian with inner function $\hat{f}_i = -\frac{(x-\mu_i)^T \Sigma_i^{-1} (x-\mu_i)}{2}$.

The parameters of Gaussian mixture models are optimized iteratively with expectation-maximization^{10,13}. The log-likelihood, \mathcal{L} , of the trained data will increase with increased number of parameters. At some point, however, adding more parameters will lead to overfitting. To select the number of Gaussian components that allows for a detailed description of the density without overfitting, we use the Bayesian information criterion (BIC)^{14,15}. BIC adds a penalty that grows with the number of parameters to the log-likelihood,

$$I_{BIC} = \log(N_{\text{points}})N_{\text{param}} - 2\mathcal{L}. \quad (3)$$

The model with smallest I_{BIC} is ultimately chosen as the one with best fit.

2.2 Extracting core states from Gaussian mixtures

Each point in a free energy landscape either belongs to a metastable core state or a transition state. To analyze the conformational ensemble, we seek well-defined core states. Such core states are easily extracted from maxima of the estimated density landscape by exploiting its functional definition. The cutoff between core state and transition state is taken at the density inflection point.

Figure 1 outlines the steps involved in the clustering method. In Figure 1 a), a plot of a two-component Gaussian mixture free energy landscape is shown. The density second-order derivative values are displayed by colors. All points with negative density second derivative

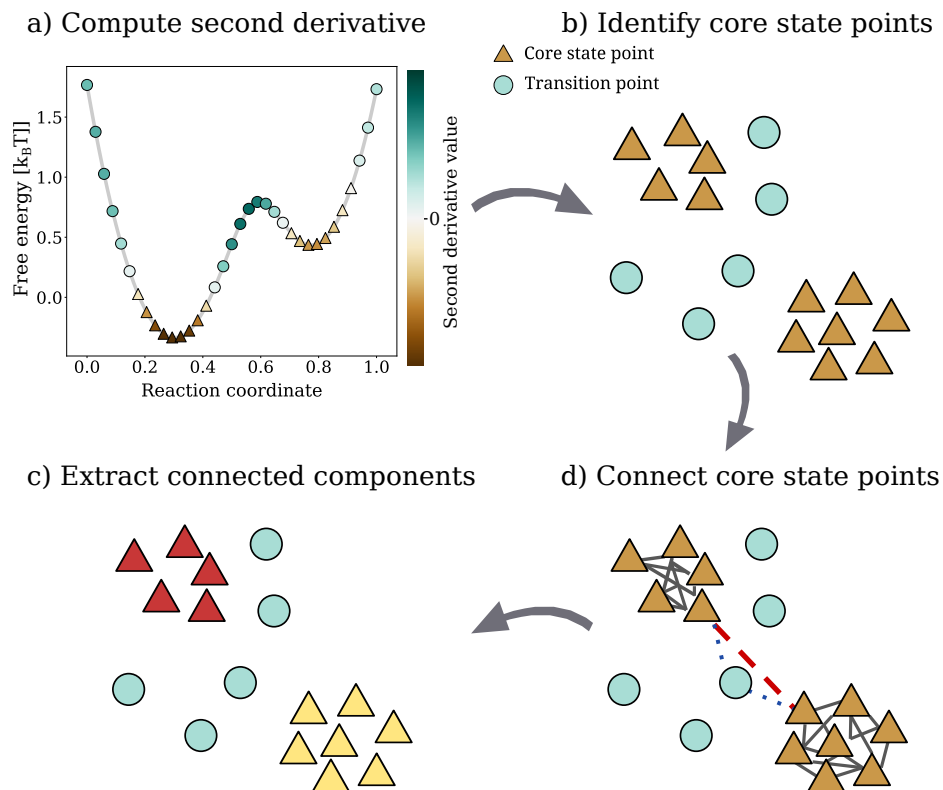


Figure 1: An illustration of the InfeCS clustering method. First, the density Hessian is computed at all points. This is used to identify core state points. Connected graphs, or components, of core state points are then built using spatial proximity between core state points and transition state points. Finally, the connected components are extracted and cluster labels are assigned to the points in these components.

values are labeled metastable core states, while the rest are labeled transition points. Islands of core state points are isolated by transition points, Figure 1 a,b). Two points within the same free energy minimum are connected by not allowing any transition point to be closer to both core state points. This creates connected components, that are extracted by assigning the same cluster label to all points within the same connected component, Figure 1 c,d).

To generalize the clustering to N_{dims} , we derive an expression for the density Hessian (matrix of second-order partial derivatives) with respect to the CVs. The partial derivative of a Gaussian mixture density, Eq. 2, with respect to the d th CV, x_d , is

$$\frac{\partial}{\partial x_d} \rho_{\mathbf{a}, \boldsymbol{\mu}, \boldsymbol{\Sigma}} = \sum_{i=1}^{N_{\text{basis}}} a_i \mathcal{N}(x | \mu_i, \Sigma_i) \frac{\partial \hat{f}_i}{\partial x_d}, \quad (4)$$

where $\frac{\partial \hat{f}_i}{\partial x_d}$ is the d th element of the inner function gradient, $\nabla \hat{f}_i = -\Sigma_i^{-1}(x - \mu_i)$. From this we obtain an expression of the (d, d') th element of the GMM density Hessian,

$$\frac{\partial^2}{\partial x_d \partial x_{d'}} \rho_{\mathbf{a}, \boldsymbol{\mu}, \boldsymbol{\Sigma}} = \sum_{i=1}^{N_{\text{basis}}} a_i \mathcal{N}(x | \mu_i, \Sigma_i) \left(\frac{\partial^2 \hat{f}_i}{\partial x_d \partial x_{d'}} + \frac{\partial \hat{f}_i}{\partial x_d} \frac{\partial \hat{f}_i}{\partial x_{d'}} \right), \quad (5)$$

where $\frac{\partial^2 \hat{f}_i}{\partial x_d \partial x_{d'}} = -\Sigma_{i, (d, d')}^{-1}$. The Hessian reflects the curvature of the landscape, such that a point belongs to a metastable core state if the Hessian is negative definite. Since the Hessian is symmetric, this is the same as all its eigenvalues being negative. Thus, the shape of the density landscape is used to label each point as core state or transition state.

Due to the continuous definition of the density, the clustering can be carried out on a grid instead of the sampled data, creating a cluster map. The sampled data points are then projected onto this cluster map by assigning a cluster label according to the closest grid point in the map. This makes the core state extraction independent of the number of data points. The grid resolution mainly affects computational efficiency, and can be determined by the user.

Transition points are left unassigned when identifying core states. For full clustering, the

transition points are first sorted in order of descending density and one-by-one assigned to the closest cluster. The highest-density point of a cluster is taken as its cluster center.

2.3 Population of states

To quantify the relative size of metastable states, we estimate the population of states, π . It reports on the probability of observing a configuration in any of the metastable states. The probability of the k th cluster is computed by integrating the density over its spanned volume, V_k ,

$$\pi_k = \int_{V_k} \rho_{\mathbf{a},\mu,\Sigma}(x) dx = \int_X I(x \in V_k) \rho_{\mathbf{a},\mu,\Sigma}(x) dx. \quad (6)$$

Here, X is the full density domain and $I(x \in V_k)$ is an indicator function which is unity if $x \in V_k$, and zero otherwise. The integral is approximated with Monte Carlo integration with 10^5 points sampled from the density landscape.

3 Methods

3.1 Conventional clustering methods

To evaluate performance and properties of InfleCS, its full clustering is compared to K-Means, agglomerative-Ward, Spectral clustering, (canonical) GMM and density peaks full clustering. Unlike InfleCS, these methods require user-specified parameters such as the number of clusters. Since the number of clusters is usually not known in real-world datasets, we use common heuristics that are based on the data. Clustering and heuristics for K-means and Agglomerative-Ward are obtained with scikit-learn¹³, while density peaks clustering is performed with a script supplied by the original authors⁷.

3.1.1 K-means

K-Means clustering is done by repeatedly assigning points to the cluster label corresponding to the nearest cluster center and updating the cluster center to the new cluster centroid. The silhouette score¹⁶ is used to select the number of clusters. A high silhouette score indicates small within cluster distances and large distances to the closest cluster, and thus a good partitioning of spherical clusters.

3.1.2 Agglomerative-Ward

Agglomerative-Ward (AW) clustering initially treats all data points as separate clusters. In each iteration, two clusters are merged to minimize within-cluster variance. This is similar to K-Means, but the cluster assignment is greedy while K-Means is optimized globally. Just as for K-Means, we determine the number of clusters with the silhouette score.

3.1.3 Spectral clustering

Spectral clustering makes use of local relationships by passing the data through a Gaussian kernel. Here, the Gaussian standard deviation is set to the maximum nearest neighbor distance. The processed data is used to create a random walk matrix from which the K largest eigenvectors are identified. The row-normalized matrix with eigenvectors represents the embedding on a K -sphere. The embedded points are then clustered with K-means.

The silhouette score is not easily applied to spectral clustering because the clustering is done in different spaces of spectral embeddings, and therefore requires a non-trivial normalization¹⁷. Instead, the largest eigengap is used to determine the number of clusters.

3.1.4 Canonical Gaussian mixture model clustering

Canonical Gaussian mixture model clustering is done by fitting a Gaussian mixture density to the data, where each Gaussian component represents a cluster. A data point is assigned

the cluster label corresponding to the component that contributes the most to its density. The number of components, and thus number of clusters, is chosen with BIC^{14,15}.

3.1.5 Density peaks

Density peaks is a recently developed density-based method, where local basis functions are used to fit a density⁷. This requires a cutoff, d_c which here is chosen so that the average number of neighbors is 2% of the number of points, as suggested by the authors⁷. After the density is estimated, cluster centers are chosen as points with significantly high density and large distance to a point with higher density. Once the centers are identified, the remaining points are assigned to the closest cluster in order of decreasing density. Density peaks allows to separate core states from transition points, but the full clustering will be used for comparison to the other methods.

The number of clusters is normally chosen based on a decision graph, aiming to pick points with relatively high density, $\rho(x)$, and large distance to the closest point of highest density, $\Delta(x)$. To pick the number of clusters automatically, the two scores are first scaled to a maximum of one, and then added to form a score for each point to be a cluster center, $s(x) = \frac{\Delta(x)}{\max\{\Delta(x)\}} + \frac{\rho(x)}{\max\{\rho(x)\}}$. To identify points with high $\Delta(x)$ and $\rho(x)$, all points are sorted in order of decreasing scores $s(x)$, and the gaps between the sorted points are calculated. A cut is made after the last consecutive point with a score gap above the median plus standard deviation of all gaps. The points above the cutoff are taken as cluster centers. Figure S1 shows examples of decision graphs and corresponding score gaps obtained for the three toy models used here.

3.2 Evaluating clustering on toy models

We use three toy models to quantify performance of the clustering methods. The first toy model is a dataset with seven Gaussian clusters. The clusters are non-equidistantly spaced and have different densities. The second dataset consists of three well-separated clusters,

among which one is clearly non-Gaussian. The third toy model attempts to mimic a real-world dataset with three poorly separated and nonlinear clusters with different densities and sizes.

Clustering quality can be assessed by computing the fraction of clustered points that originate from the same true class. This gives the homogeneity score. A maximum homogeneity score is reached when the clustering is perfect, but also if points from one true class are divided into more than one cluster. A remedy is to instead report on the fraction of points from a true class that belongs to a single cluster, the completeness score. However, a perfect score is then obtained if points from different true classes are assigned to the same cluster. Since this is complementary to the homogeneity score, we use the average of the homogeneity and completeness scores, the so called V-measure^{13,18}, to evaluate clustering quality. It gives a score between zero and one, where one indicates perfect clustering. To gather statistics, we repeat the sampling, clustering and V-measure evaluation 50 times for each toy model and clustering method.

3.3 Molecular simulations of Ca²⁺-bound Calmodulin

We apply InflexCS to an ensemble of Ca²⁺-bound Calmodulin (CaM) configurations¹⁹. CaM consists of 148 residues arranged in eight helices and three domains; the N-terminal and C-terminal lobes, as well as the flexible linker between them. The two lobes have two EF-hand motifs each, enabling CaM to bind four Ca²⁺ ions. The helices are named from A to H, from N- to C-terminus. In the Ca²⁺-bound state, CaM commonly adopts a dumbbell shaped conformation with exposed hydrophobic clefts. The exposed hydrophobic clefts facilitate binding to, and thus regulating, a wide range of target proteins, including ion channels and kinases.

We investigate the conformational dynamics of Ca²⁺-bound CaM with 460 ns already published²⁰ replica exchange solute tempering (REST) simulations^{21,22}. To analyze CaM, we project the protein heavy atom coordinates onto two collective variables. The first CV,

difference in distribution of reciprocal interatomic distances (DRID)²³, reflects on the global conformational change relative the initial crystal structure²⁴. In short, the distribution of inverse distances between C_α atoms are used to extract three features for each residue; the mean, the square root of the second central moment, and the cubic root of the third central moment. Thus, each frame j is described by a feature matrix, $\mathbf{v}_j \in \mathbb{R}^{3 \times N_{\text{Residues}}}$. The difference to the initial structure with features \mathbf{v}_0 is computed as the average residue feature distance

$$\text{DRID}_j = \frac{1}{3N_{\text{Residues}}} \sum_{n=1}^{N_{\text{Residues}}} \|\mathbf{v}_j^n - \mathbf{v}_0^n\|. \quad (7)$$

The second CV, backbone dihedral angle correlation (BDAC)¹, reports on secondary structure changes in the linker relative the initial structure,

$$\text{BDAC}_j = \frac{1}{4N'_{\text{Residues}}} \sum_{n=1}^{N'_{\text{Residues}}} (2 + \cos(\varphi_j^n - \varphi_0^n) + \cos(\psi_j^n - \psi_0^n)). \quad (8)$$

Here, φ_j^n and ψ_j^n are the backbone dihedral angles of linker residue n in frame j . MDtraj²⁵ was used to compute DRID feature vectors and backbone dihedral angles.

4 Results and discussion

4.1 Toy models

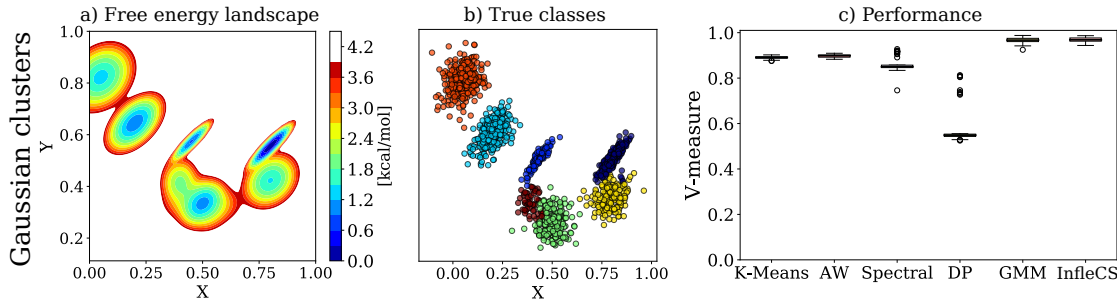


Figure 2: Performance of all clustering methods on a toy model dataset with Gaussian clusters. a) The true free energy landscape of the toy model, b) an example of sampled data and its true clustering and c) the V-measure scores for the six clustering methods.

The first toy model consists of Gaussian clusters generated from the free energy landscape in Figure 2 a). An example of sampled data with true cluster labels is displayed in Figure 2 b), and performances of the different clustering methods on this toy model are shown in Figure 2 c). Because the clusters are Gaussian and have similar spatial size, most methods perform well. Specifically, GMM and InfleCS provide close to perfect clustering. Density peaks, on the other hand, performs poorly. The problem stems from the varying cluster densities, which are evident in the free energy landscape, Figure 2 a). This adds complexity to the density peaks decision graph, Figure S1 a), making it difficult to extract the correct cluster centers.

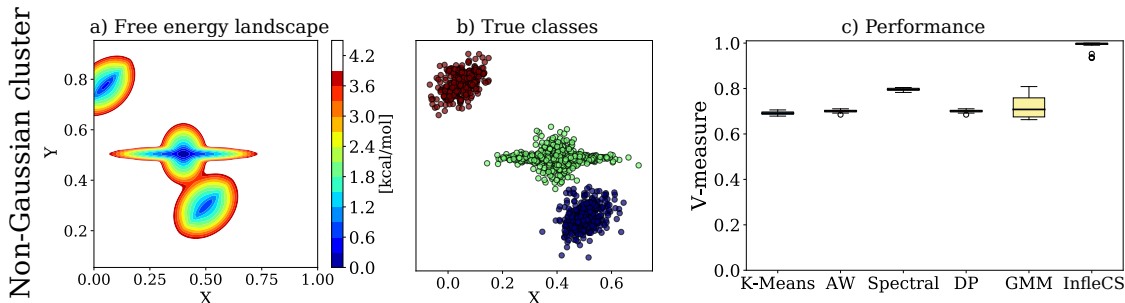


Figure 3: Performance of all clustering methods on a toy model dataset with one non-Gaussian cluster. a) The true free energy landscape of the toy model, b) an example of sampled data and its true clustering and c) the V-measure scores for the six clustering methods.

To investigate the impact of cluster shapes on clustering performance, a second toy model with one non-Gaussian cluster is introduced, Figure 3 a,b). This toy model highlights how GMM, K-means and agglomerative-Ward fail because their intrinsic assumptions are not met, Figure 3 c). Density peaks, on the contrary, performs better than on the first toy model because the clusters have similar density. Interestingly, spectral clustering has similar performance as on the first toy model while InfleCS performs almost perfectly. These methods extract clusters with graphs based on local relationships between data points, and are therefore less sensitive to varying cluster shapes.

The third toy model mimics data projected from a high dimensional to a low dimensional space. The clusters are poorly separated and nonlinear. By mere inspection of the scattered

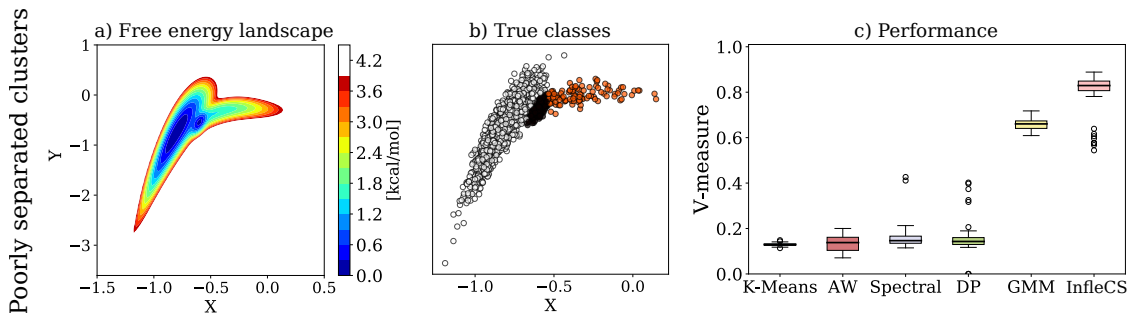


Figure 4: Performance of all clustering methods on a toy model dataset with poorly separated and non-linear clusters. a) The true free energy landscape of the toy model, b) an example of sampled data and its true clustering and c) the V-measure scores for the six clustering methods.

data, Figure 4 b), it is difficult to identify the clusters. The free energy landscape, however, clearly shows three states, Figure 4 a). Because the clusters are poorly separated and of different spatial sizes, the geometric clustering methods completely fail, Figure 4 c). In addition to this, density peaks has a low clustering quality due to the spatially small-sized clusters of relatively low density. This makes the density peaks decision graph far from simple to interpret, Figure S1 c). The cluster centers chosen in density peaks require high density clusters. By simply decreasing the weight on density to half in the density peaks gap cut score, density peaks performs slightly better, Figure S2. However, it never reaches the same quality as InfleCS. Moreover, a good weighting is arbitrary and unknown in real datasets. Despite the poorly separated states with different density and sizes, it is clear that InfleCS manages to provide high quality clustering, Figure 4 c). Thus, it is the only method in this set that successfully clusters all toy model datasets.

4.2 Application to Ca^{2+} -bound Calmodulin

The estimated free energy landscape of CaM along the two CVs and the corresponding InfleCS clustered data are shown in Figure 5 a,b). As expected, InfleCS correctly identifies the metastable states within the free energy landscape. The core state probabilities, Figure 5 c), show that the sixth state is the most common state in this dataset. Representative structures

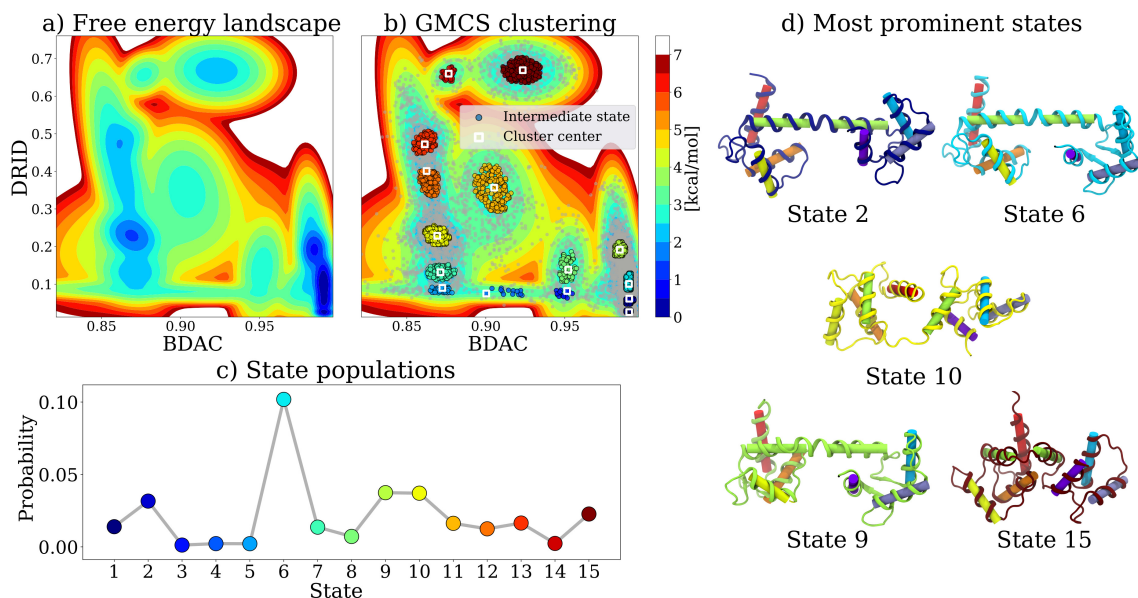


Figure 5: a) The estimated free energy landscape of the CaM conformational ensemble along the two CVs. b) The identified core states based on the estimated density, colored by cluster labels. Transition points are shown as gray dots. c) The state populations. d) Structures of each cluster center. The ribbons are colored according to the cluster the structure belongs to, while the cylinders, helix A to H, are colored according to a rainbow. Structures are visualized with VMD²⁶.

of the most populated states are shown in Figure 5 d). The most common structure is in a canonical dumbbell conformation, but we also identify two different compact conformations among these well-populated states, namely state 10 and 15. Compact states similar to state 15 have been identified in previous MD datasets^{27–30} as well as in an experimental structure³¹.

With the estimated free energy landscape available, we can infer possible pathways between states and thus understand how the states are connected. For example, the tenth state is a relatively highly populated compact state with helix A collapsed onto the linker. By mere inspection of the representative structures, it is not obvious how CaM transitions to this state from the canonical conformation (state 6). A possible pathway between the canonical and compact state in the free energy landscape goes through state 8, Figure 6 a). The representative structures corresponding to cluster centers, Figure 6 b), indicate that the transition likely occurs through a twisting motion of the two lobes around the linker and

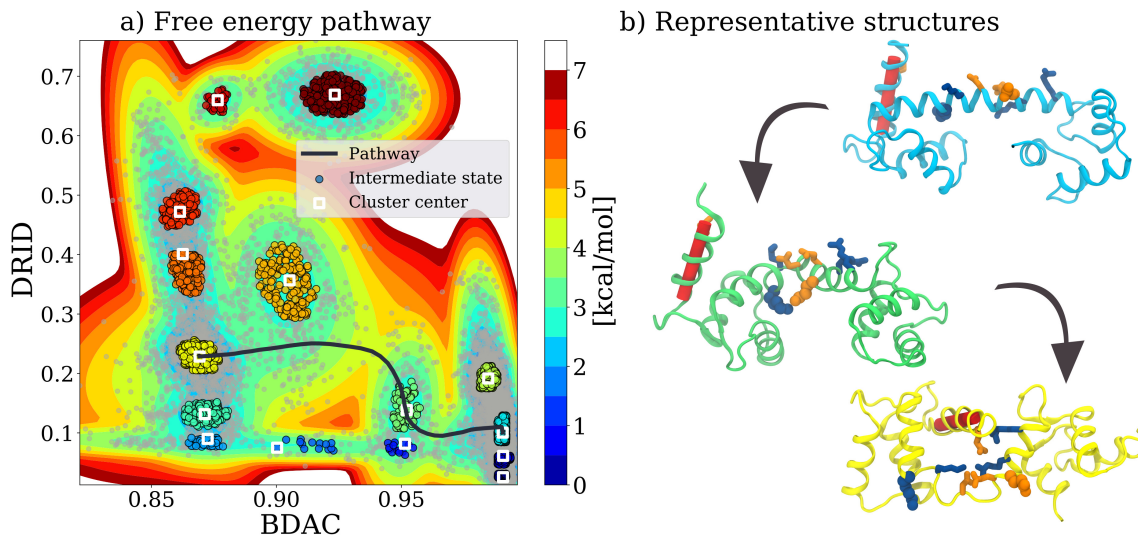


Figure 6: a) A free energy pathway between the most common state 6 to the compact state 10. The path goes through state 8. b) Representative structures of the involved states. The ribbons are colored according to the cluster the structure belongs to, while the cylinder, helix A, is colored red. The positively (negatively) charged residues that participate in salt-bridge formation and breaking are shown with blue (orange) sticks (GLU11, LYS77, ASP80, GLU83, ARG86, ARG90). LYS75 and GLU84 are shown with blue and orange spheres, respectively. Structures are visualized with VMD²⁶.

breaking of the linker helix.

Early MD simulations and experimental studies of CaM suggest that destabilization of the linker helix is driven by electrostatic interactions^{28,29,32-34}. We therefore study salt bridges in the three core state ensembles along the pathway. Going from the canonical to the intermediate state, the linker helix breaks which enables formation of a stabilizing salt bridge between LYS75 and GLU84, Figure 6 b) and S3 a,b). To transition to the compact state, GLU11 is likely recruited by LYS77, which breaks the LYS75-GLU84 salt bridge in favor of a new charged cluster with salt bridges between LYS77-GLU83, ASP80-ARG86, GLU11-ARG86 and GLU11-ARG90, Figure 6 b) and Figure S3 c). LYS75 is a common target-protein binding residue³⁵. Thus, the salt bridge formations in this compact state that expose LYS75 may promote initiation of long-ranged interactions with target proteins.

5 Conclusions

We presented InfleCS, a clustering method that uses the shape of an estimated Gaussian mixture density to identify metastable core states. The method was shown to consistently outperform other common clustering methods on three toy models with different properties.

The advantages with InfleCS for free energy landscape clustering are five-fold. First, clusters are identified at density peaks, which guarantees that clusters are metastable states. Second, core state boundaries identified by density second derivatives are well-defined. Third, clusters are constructed by building graphs, thus making minimal assumptions about cluster shapes. Fourth, because the clustering method naturally involves density and free energy landscape estimation, it is possible to derive pathways between states and thus understand fundamental mechanisms. Finally, the number of clusters is naturally determined by the number of density peaks in the landscape and therefore requires no a priori system knowledge.

By applying InfleCS to a conformational ensemble of Ca^{2+} -bound CaM, we identified a possible pathway from the canonical to a compact state through a twisting motion of the two lobes followed by salt bridge breaking and formation. This pathway highlights electrostatically driven structural rearrangements that may allow CaM to bind to a wide range of target proteins.

Acknowledgement

The simulations were performed on resources provided by the Swedish National Infrastructure for Computing (SNIC) at PDC Centre for High Performance Computing (PDC-HPC). This work was supported by grants from the Science for Life Laboratory.

Supporting Information Available

The following files are available free of charge. The code and tutorial for estimating free energy landscapes and cluster with InfeCS are available free of charge at http://www.github.com/delemottelab/tutorial_FE_clustering.

References

- (1) Westerlund, A. M.; Harpole, T. J.; Blau, C.; Delemotte, L. *J. Chem. Theory and Comput.* **2017**,
- (2) Sorensen, T. *Biol. Skr.* **1948**, *5*, 1–34.
- (3) Sneath, P. H. A. *Microbiol.* **1957**, *17*, 201–226.
- (4) Ward, J. H. *J. Am. Stat. Assoc.* **1963**, *58*, 236–244.
- (5) MacQueen, J. Some methods for classification and analysis of multivariate observations. 5th Berkeley Symp. Math. Stat. Prob. 1967.
- (6) Ng, A. Y.; Jordan, M. I.; Weiss, Y. On Spectral Clustering: Analysis and an Algorithm. Proc. 14th Int. Conf. Neural Inf. Proc. Sys.: Nat. Synth. Cambridge, MA, USA, 2001; pp 849–856.
- (7) Rodriguez, A.; Laio, A. *Science* **2014**, *344*, 1492–1496.
- (8) Sittel, F.; Stock, G. *J. Chem. Theory Comput.* **2016**, *12*, 2426–2435.
- (9) Ester, M.; Kriegel, H.-P.; Sander, J.; Xu, X. A Density-based Algorithm for Discovering Clusters in Large Spatial Databases with Noise. Proc. Sec. Int. Conf. Knowl. Discovery Data Min. 1996; pp 226–231.
- (10) Dempster, A. P.; Laird, N. M.; Rubin, D. B. *J. Royal Stat. Soc. B* **1977**, *39*, 1–38.
- (11) Bishop, C. M. *Pattern Recognit. and Mach. Learn.*; Springer: New York, 2011.
- (12) Hennig, C. *Adv. Data Anal. Classif.* **2010**, *4*, 3–34.
- (13) Pedregosa, F.; Varoquaux, G.; Gramfort, A.; Michel, V.; Weiss, R.; Dubourg, V.; Vanderplas, J.; Passos, A.; Cournapeau, D.; Brucher, M.; Perrot, M.; Duchesnay, E. *J. Mach. Learn. Res.* **2011**, *12*, 2825–2830.

- (14) McLachlan, G. J.; Rathnayake, S. *Wiley Interdiscip. Rev.: Data Min. Knowl. Discovery* **2014**, *4*, 341–355.
- (15) Schwarz, G. *Ann. Statist.* **1978**, *6*, 461–464.
- (16) Rousseeuw, P. J. *J. Comput. Appl. Math.* **1987**, *20*, 53 – 65.
- (17) Ponzoni, L.; Polles, G.; Carnevale, V.; Micheletti, C. *Structure* **2015**, *23*, 1516–1525.
- (18) Rosenberg, A.; Hirschberg, J. V-Measure: A Conditional Entropy-Based External Cluster Evaluation Measure. Proc. 2007 Jt. Conf. Empirical Methods Nat. Language Proc. Comput. Nat. Language Learn. 2007; pp 410–420.
- (19) Stevens, F. C. *Can. J. Biochem. Cell Biol.* **1983**, *61*, 906–910.
- (20) Westerlund, A. M.; Delemotte, L. *PLoS Comput. Biol.* **2018**, *14*, 1–27.
- (21) Wang, L.; Friesner, R. A.; Berne, B. J. *J. Phys. Chem. B* **2011**, *115*, 9431–9438.
- (22) Bussi, G. *Mol. Phys.* **2014**, *112*, 379–384.
- (23) Zhou, T.; Caffisch, A. *J. Chem. Theory Comput.* **2012**, *8*, 2930–2937.
- (24) Babu, Y. S.; Bugg, C. E.; Cook, W. J. *J. Mol. Biol.* **1988**, *204*, 191–204.
- (25) McGibbon, R.; Beauchamp, K.; Harrigan, M.; Klein, C.; Swails, J.; Hernandez, C.; Schwantes, C.; Wang, L.-P.; Lane, T.; Pande, V. *Biophys. J.* **2015**, *109*, 1528–1532.
- (26) Humphrey, W.; Dalke, A.; Schulten, K. *J. Mol. Graphics* **1996**, *14*, 33–38.
- (27) Aykut, A. O.; Atilgan, A. R.; Atilgan, C. *PLoS Comput. Biol.* **2013**, *9*, e1003366.
- (28) Fiorin, G.; Biekofsky, R. R.; Pastore, A.; Carloni, P. *Proteins: Struct., Funct., Bioinf.* **2005**, *61*, 829–839.
- (29) Shepherd, C. M.; Vogel, H. J. *Biophys. J.* **2004**, *87*, 780–791.

- (30) Wriggers, W.; Mehler, E.; Pitici, F.; Weinstein, H.; Schulten, K. *Biophys. J.* **1998**, *74*, 1622 – 1639.
- (31) Fallon, J. L.; Quioco, F. A. *Structure* **2003**, *11*, 1303–1307.
- (32) Spoel, D. V. D.; Groot, B. L. D.; Hayward, S.; Berendsen, H. J. C.; Vogel, H. J. *Protein Sci.* **1996**, *5*, 2044–2053.
- (33) Torok, K.; Lane, A. N.; Martin, S. R.; Janot, J. M.; Bayley, P. M. *Biochemistry* **1992**, *31*, 3452–3462, PMID: 1554727.
- (34) Kataoka, M.; Persechini, A.; Tokunaga, F.; Kretsinger, R. H. *Proteins: Struct., Funct., and Bioinf.* **1996**, *25*, 335–341.
- (35) Villarroel, A.; Taglialatela, M.; Bernardo-Seisdedos, G.; Alaimo, A.; Agirre, J.; Alberdi, A.; Gomis-Perez, C.; Soldovieri, M. V.; Ambrosino, P.; Malo, C.; Areso, P. *J. Mol. Biol.* **2014**, *426*, 2717–2735.

Supplementary material: Clustering Free Energy Landscapes with Gaussian Mixtures

Annie M. Westerlund and Lucie Delemotte*

Science for Life Laboratory, Department of Applied Physics, KTH Royal Institute of Technology, Box 1031, SE-171 21 Solna

E-mail: lucie.delemotte@scilifelab.se

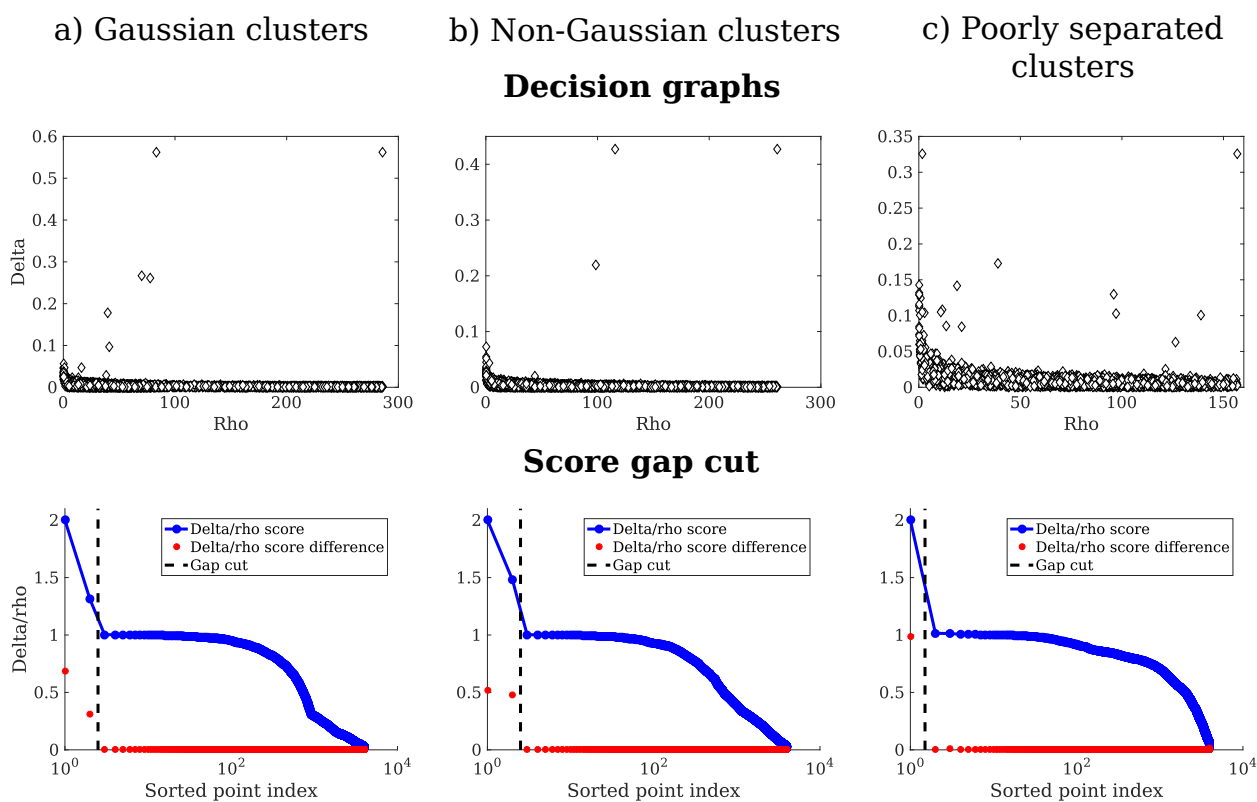


Figure S1: Examples of density peaks decision graphs obtained for the three toy models, and the corresponding gap score cutoffs.

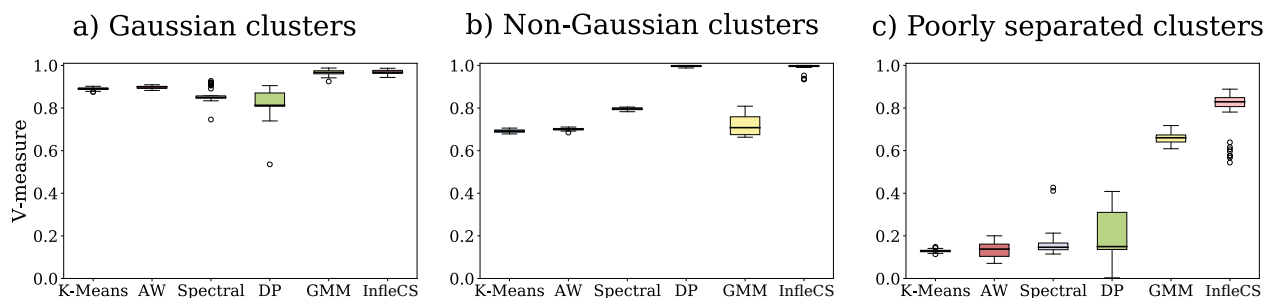


Figure S2: V-measure scores of clustering methods with density peaks cluster center decision based on down-weighted density importance.

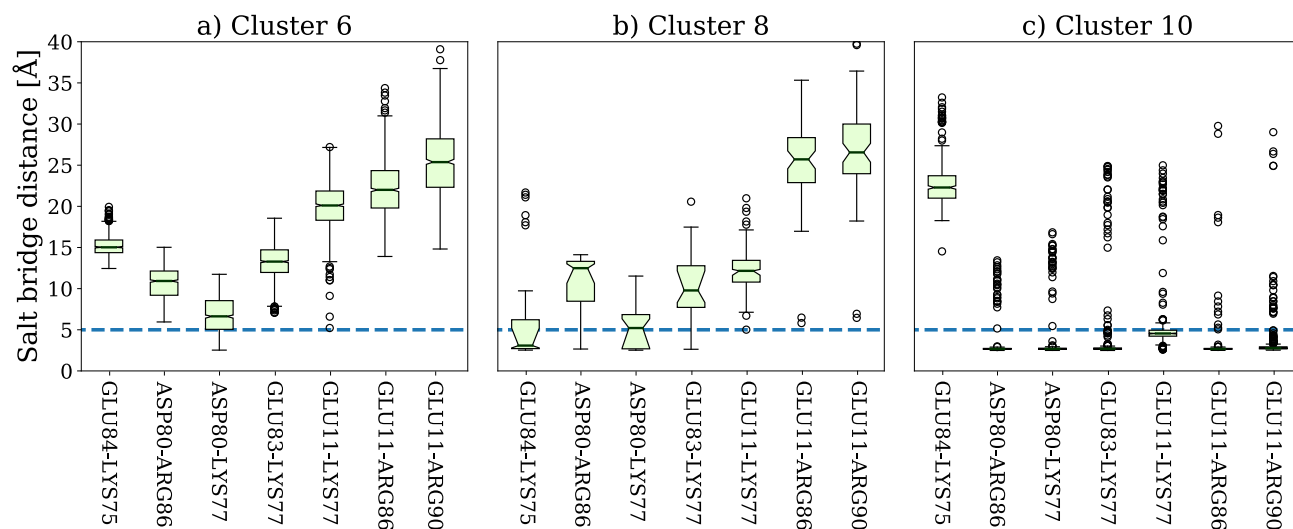


Figure S3: Distances between side chain N and O of selected residues. a) Salt bridge distances of cluster 6. b) Salt bridge distances of cluster 8. c) Salt bridge distances of cluster 10.